Sub-nucleolar trafficking of Hendra virus matrix protein is regulated by ubiquitination and oligomerisation

Stephen M. Rawlinson[1*#], Tianyue Zhao[1*], Cassandra T. David[1], Patrick F. Veuglers[1,2], Ashley M. Rozario[3], Toby D.M. Bell[2] and Gregory W. Moseley[1#]

[1] Department of Microbiology, Biomedicine Discovery Institute, Monash University, 19 Innovation Walk (Bldg 76), Clayton Campus, Victoria 3800, Australia.

[2] School of Chemistry, Monash University, Clayton, Victoria 3800, Australia.

[3] Department of Rural Clinical Sciences, La Trobe Institute for Molecular Science, La Trobe University, Bendigo, Victoria 3552, Australia.

* SMR and TZ contributed equally to this work.

Correspondence should be addressed to: SMR (stephen.rawlinson@monash.edu) and GWM (greg.moseley@monash.edu).

ABSTRACT

Hendra virus (HeV) is a highly pathogenic member of the Henipavirus genus (order *Mononegavirales*), the replication cycle of which occurs primarily in the cytoplasm. The HeV matrix protein (HeV M) plays critical roles in viral assembly and budding at the plasma membrane, but also undergoes nuclear/nucleolar trafficking, to accumulate in nucleoli early in infection and, later, localise predominantly at the plasma membrane. Previously we found that HeV M protein targets specific sub-nucleolar compartments (corresponding to the FC-DFC (fibrillar centre (FC)/dense fibrillar component (DFC)) where it interacts with the nucleolar protein Treacle and modulates rRNA biogenesis by subverting the host nucleolar DNA damage response, indicating the importance of specific sub-nucleolar trafficking to infection. However, the mechanisms underlying targeting and movement between sub-nucleolar compartments by viral or cellular proteins remain poorly defined. Here, we assessed the molecular regulation of HeV M protein nucleolar/sub-nucleolar trafficking, finding that HeV M localizes into Treacle-enriched FC-DFC early after expression, but this localization is progressively depleted through relocalization to the surrounding granular component (GC) of the nucleolus. Analysis using mutated M proteins and pharmacological modulation of ubiquitination indicate that this dynamic localization is regulated by ubiquitination and oligomerisation, with ubiquitination required for retention of HeV M in Treacle-enriched sub-nucleolar compartments, and oligomerisation required for egress. To our knowledge, this study provides the first direct insights into the dynamics and mechanisms of viral protein trafficking between sub-nucleolar compartment, shedding light on the intricate interplay between HeV M and host cell factors during infection.

INTRODUCTION

The nucleolus comprises a highly multifunctional structure with long established roles in ribosome biogenesis, as well as roles in cell cycle regulation, the DNA damage response (DDR), cellular stress responses, and signal recognition particle assembly [1, 2]. The nucleolus was recently shown to be a membrane-less organelle (MLO) comprising at least three immiscible liquid condensates that are formed by liquid-liquid phase separation (LLPS) [3]. The three components are the fibrillar centre (FC), dense fibrillar component (DFC) and granular component (GC). The FC is surrounded by the DFC to form functional units (FC-DFC), which are embedded within the GC (Fig. 1A) [4]. These compartments play distinct roles, including assembling a pipeline for the key steps of ribosome biogenesis.

Consistent with its multifunctionality, the nucleolus is a common target of diverse viruses [5-7]. This targeting is proposed to enable viral exploitation of diverse processes to usurp host cell biology and/or facilitate virus replication [5-7]. Despite the prevalence of viral protein nucleolar targeting, functional outcomes generally remain poorly understood. The potential nucleolar functions of viral proteins are of particular interest with respect to RNA viruses that typically have limited coding capacity and replicate their genomes in the cytoplasm, but nevertheless target specific proteins to nucleoli. These include the highly pathogenic non-segmented negative sense RNA viruses (nsNSVs) Hendra (HeV) and Nipah (NiV) viruses (genus *Henipavirus*, family *Paramyxoviridae*), the matrix (M) protein of which localizes to the nucleus and nucleolus during infection [8-11].

Henipavirus M proteins form stable homodimers, and play critical roles in virus assembly in the cytoplasm and in budding at the plasma membrane, which involves the formation of oligomers [12, 13]. The subcellular localization of M protein is dynamic, being nucleolar early in infection before exiting the nucleolus/nucleus and accumulating at the plasma membrane for assembly/budding [8-11]. Interestingly, transit through the nucleolus is reported to be a prerequisite for M protein to fulfill assembly and budding functions, suggestive of a regulatory role of nucleoli in viral release [10, 11]. Genetic screens have indicated the importance of nucleolar proteins in infection, and proteomic datasets suggest that M protein interacts with multiple nucleolar proteins [8, 10, 14, 15]. However, potential intranucleolar roles of HeV M protein remained unresolved until the identification of a novel nucleolar function whereby HeV M localises to a sub-nucleolar compartment corresponding to the FC-DFC, where it interacts with Treacle protein and impairs ribosomal RNA (rRNA) biogenesis [14]. This process appears to be mediated by mimicry of a cellular process that normally occurs during a DDR. Thus HeV M subcellular trafficking underpins key functions of HeV M. However, how this trafficking is regulated, particularly between sub-nucleolar compartments and other regions of the cell remains unresolved. Indeed, the mechanisms regulating trafficking of proteins in general between sub-nucleolar liquid condensates is poorly understood, with no prior studies to our knowledge, for any viral protein.

Previously we showed that substitution of residue K258 in HeV M for alanine (HeV M K258A) impairs FC-DFC localisation/Treacle-binding and DDR modulation/budding activity, without preventing localization to the GC, where HeV M K258A accumulates [14]. K258 forms part of a bipartite nuclear localization sequence (NLS; often referred to as ‘NLS2’; M contains at least two

NLSs; NLS1 is located at residues 82-87 [16, 17]) and can be ubiquitinated (Fig. 2A) [10, 11] and it has been proposed that the M protein enters the nucleus via the NLS and accumulates within nucleoli before exiting the nucleolus and nucleus (mediated by a nuclear export sequence (NES)); exit of the nucleolus/nucleus is reported to be triggered by ubiquitination at K258 by an unidentified ubiquitin ligase [18]. However, this model was proposed prior to the description of the functionally important localization of HeV M to sub-nucleolar compartments. As a result, the coordination and regulation of various trafficking steps, including trafficking within the nucleolus, remain undefined.

In this study, we examine the regulation of HeV M protein trafficking between the FC-DFC and GC finding that K258 ubiquitination plays a crucial role. Interestingly, ubiquitination exerts opposing effects on sub-nucleolar and nucleocytoplasmic localization, suppressing exit from the FC-DFC to the GC while being required for egress from the nucleolus/nucleus. Furthermore, mutations affecting HeV M oligomerization indicated that oligomerization is necessary for FC-DFC egress. These findings provide new insights into the complex interplay of ubiquitination and oligomerization in HeV M protein nuclear/nucleolar transit and roles in modulation of host cell biology, viral assembly and budding.

RESULTS

Ubiquitination is important to sub-nucleolar trafficking of HeV M.

Previously the HeV M residue K258 (and equivalent residues in other henipaviruses) was shown to be mono-ubiquitinated [10, 11], with the proteasome/ubiquitination inhibitor, MG132, shown to cause nuclear and nucleolar retention of HeV and NiV M proteins, and inhibit nuclear export and viral-like particle (VLP) production by NiV M proteins [10, 11].

To explore the possibility that ubiquitination regulates trafficking between sub-nucleolar condensates, we examined the effect of MG132 treatment on the sub-nucleolar localization of HeV M proteins using confocal laser scanning microscopy (CLSM) of living HeLa cells expressing GFP-fused wild-type (WT) HeV M (GFP-HeV M) (Fig. 1B). As expected [10, 11], MG132 treatment resulted in nuclear accumulation of HeV M protein (Fig. 1B), which was confirmed by a significant increase in the nuclear to cytoplasmic fluorescence ratio (Fn/c) (Fig. 1C), consistent with impaired nuclear export [10, 11]. However, we also observed a reduction in FC-DFC targeting by HeV M protein following MG132 treatment (Fig. 1B), confirmed by a reduced ratio of fluorescence intensity of the FC-DFC compared with the GC ($F_{FC\text{-}DFC/GC}$) (Fig. 1D), an increase in GC fluorescence (Fig. 1E), and a decrease in the number of cells displaying FC-DFC accumulation (Fig. 1F). These findings suggest that ubiquitination promotes the accumulation of HeV M protein within the FC-DFC, whereas reduced ubiquitination leads to accumulation within the GC.

Conservative substitution of K258 to R reduces FC-DFC targeting by HeV M.

We previously showed that K258A mutation in HeV M protein (HeV M K258A) abolishes its targeting to the FC-DFC, resulting in accumulation within the GC and loss of binding to the FC-

DFC-enriched protein, Treacle [14]. This suggested that K258 forms part of a targeting signal due to its positive charge and/or affects sub-nucleolar localization due to its ubiquitination [10, 11]. The above data (Fig. 1) indicate an importance for ubiquitination in the retention of HeV M within the FC-DFC. To examine whether this relates to ubiquitination at K258 specifically, we compared the effects on subcellular localization of HeV M by the K258A (which removes the positive charge and ubiquitination site) and K258R (which retains positive charge but lacks the ubiquitination site) (Fig. 2A). Previous studies on equivalent mutations in NiV M protein indicated that the positive charge is important to function of the NLS, while ubiquitination regulates nuclear export [11].

CLSM analysis of cells expressing GFP-fused HeV M WT, K258A or K258R variants (Fig. 2B), indicated sub-nucleolar accumulation of WT M protein in c. 90% of cells, consistent with localization to FC-DFC (Fig. 2C). As expected [14], HeV M K258A protein lost FC-DFC localization and accumulated within the GC (Fig. 2B). In contrast, HeV M K258R displayed an intermediate phenotype, with a substantial proportion of cells (c. 60%) showing FC-DFC accumulation similar to WT and the remainder lacking FC-DFC accumulation similar to K258A (Fig. 2B, C). Consistent with this, the $F_{FC\text{-}DFC/GC}$ ratio for HeV M K258A (c. 1.0) was significantly lower than WT (c. 1.8), while HeV M K258R showed an intermediate phenotype (c. 1.4), due to the presence of WT- and K258A-like populations; notably, the FC-DFC localization of the WT-like population was significantly reduced compared with the genuine WT protein ($p < 0.01$) (Fig. 2D).

Dynamic localization of HeV M in sub-nucleolar compartments is regulated by K258.

The effects of the K258 mutation on HeV M protein accumulation in FC-DFC suggest potential impacts on a targeting sequence and/or affinity for specific components within these compartments. K258 in NiV M protein is proposed to be part of a NLS, which typically consist of short stretches of basic residues, and several basic residues (R244, R245, R256, R257, K258 in NiV M) highly conserved among henipavirus M proteins [10, 11]. Thus K258 may play a crucial role in nuclear import through the NLS and contribute to an overlapping targeting sequence for nucleoli/sub-nucleolar FC-DFC [11, 17]. Previous data indicated that ubiquitination dynamically regulates nuclear localization of HeV M [10, 11]. Furthermore, henipavirus M protein undergoes dynamic and temporal regulation of localization during infection, being nuclear/nucleolar early in infection, before nucleolar exit/nuclear export, and eventual accumulation/budding at the plasma membrane [9, 11]. We thus speculated that the observed differences in FC-DFC localization between HeV M WT and the K258 mutants (assessed at 24 h post transfection (p.t.) in Fig. 1 and Fig. 2) might be attributable to dynamic regulation of the various M protein trafficking signals.

To investigate this, we assessed sub-nucleolar localization of WT and mutant HeV M proteins at time points p.t. from 8 h to 72 h (Fig. 3A-C). The WT HeV M protein exhibited clear accumulation in FC-DFC (typically multiple structures in each nucleolus) at 8 h p.t. (c. 85% of cells), and FC-DFC localization progressively diminished over the course of the experiment, accompanied by a more diffuse GC distribution with only around 10% of cells exhibiting M protein accumulation in multiple FC-DFC at 72 h p.t. (Fig. 3D). This is consistent with a dynamic interaction whereby HeV M initially enters the FC-DFC and then undergoes gradual egress to the GC. Measurement of the $F_{FC\text{-}DFC/GC}$ confirmed a progressive loss of FC-DFC localization (Fig. 3E).

Consistent with roles of K258 in NLS activity of NiV M protein [10], nuclear localization of HeV M K258A was reduced compared with WT at 8 and 16 h p.t., supporting its involvement in nuclear import (Fig. 3F; Fn/c c. 2 for WT, c.f. c. 1 for K258A at both timepoints). Further analysis revealed that the reduction in nuclear localization of the K258A mutant was due to a significant proportion of cells showing higher fluorescence intensity in the cytoplasm (Fc) than in the nucleus (Fn) at early time points, in contrast to the WT and K258R (Fig. 3G; c. 50-60% of cells showed Fn > Fc for K258A between 8-24 h p.t., in contrast to WT, with > 85% of cells shown Fn > Fc at all timepoints). However, over time, the K258A mutant gradually exhibited nuclear import similar to the WT and K258R, with nearly 100% of cells showing Fn > Fc at 48 and 72 h p.t., suggesting a delayed nuclear import compared to the other variants.

Despite reduced nuclear accumulation at early time points, HeV M K258A was strongly nucleolar at all time points, indicative with reduced nucleolar egress. However, no accumulation in FC-DFC was observed at any time point, and some images indicated absence of fluorescence from these structures (e.g. white arrow, 48 h p.t., Fig. 3B). Thus, HeV M protein can specifically partition between sub-nucleolar phase-separated compartments, dependent on K258, and this is independent of global level of accumulation in the nucleus.

In contrast to K258A, HeV M K258R accumulated to higher levels in the nucleus than the cytoplasm at early time points (Fig. 3B, upper panels and 3F), similar to WT M. This is consistent with a requirement for the positive charge in the NLS for efficient nuclear import, as reported for NiV M protein [11, 17]. Additionally, HeV M K258R accumulated to very high levels in the nucleus, consistent with an impaired nuclear export mechanism [10, 11]. HeV M K258R also

showed clear FC-DFC localization in Treacle-enriched compartments at 8 h p.t. (Fig. 3C), similar to WT HeV M protein, followed by loss of FC-DFC localization over time. Thus, the presence of a basic residue at position 258 is necessary for initial entry and accumulation within the FC-DFC.

While FC-DFC localization of WT and K258R HeV M protein diminished following the initial accumulation, the apparent rate of loss was greater for HeV M K258R, such that by 24 h p.t. (Fig. 3A, C) c. 25% of HeV M K258R-expressing cells displayed FC-DFC localization compared with c. 60% for WT HeV M. By 48 and 72 h p.t. < 5% and 0%, respectively, of HeV M K258R-expressing cells displayed FC-DFC localization, and nucleoli with apparent exclusion from FC-DFC structures were apparent (e.g. 48 h p.t., Fig. 3C, white arrows), similar to those in cells expressing HeV M K258A. The $F_{FC\text{-}DFC/GC}$ ratio confirmed a significant decrease in FC-DFC localization by both HeV M WT and K258R over the course of the experiment, with a more rapid decrease for the latter (Fig. 3E). Thus, it appears that HeV M localises initially to the FC-DFC, dependent primarily on the presence of a positive charge at position 258. HeV M then relocalizes to the GC, and this process is accelerated in HeV M containing the K258R substitution that cannot be ubiquitinated, indicating that ubiquitination causes retention into the FC-DFC.

FC-DFC accumulation is enhanced by inhibition of oligomerization of HeV M protein.

Protein oligomerization has been associated with regulation of subcellular localization, including nuclear import and export of proteins such as p53 [19] and signal transducer and activator of transcription (STAT) proteins [20]. Moreover, oligomerization is implicated in the formation of MLOs through LLPS [21, 22]. Based on the crystal structure of HeV M protein, residue R57 of HeV M has been implicated in oligomerization *via* packing of HeV M dimers [13]. Mutation of

R57 to D or E impairs the formation of VLPs by M protein, suggesting roles for oligomerization in the assembly and budding processes [13]. Additionally, it was hypothesized that ubiquitin modification at K258 may be necessary for M protein oligomerization [18]. Assembly and budding is also dependent on K258 [10, 11], suggesting that nuclear and nucleolar localization/trafficking, and budding are intrinsically linked and/or involve coordinated regulation. However, the specific roles of oligomerization in HeV M nuclear/nucleolar trafficking have not been investigated.

To examine this we analysed the localisation of HeV M WT or R57D as above, which indicated pronounced accumulation of HeV M R57D into the FC-DFC compared to the WT protein (Fig. 4A). The Fn/c was not significantly different between HeV M WT and R57D indicating similar function of the nuclear trafficking signals (Fig. 4B). However, the ratio of nucleolar to nuclear fluorescence (Fnu/n) (Fig. 4C) and $F_{FC\text{-}DFC/GC}$ (Fig. 4D) was significantly increased for HeV M R57D compared to WT HeV M protein. Thus, R57D enhances the accumulation of HeV M in the FC-DFC, consistent with a role for oligomerization in regulating the localization of HeV M to nucleolar condensates.

Accumulation of HeV M protein in the FC-DFC correlates with inhibitory function toward rRNA biogenesis and with binding to Treacle.

HeV M protein accumulation in FC-DFC enables subversion of the nucleolar DDR pathway through targeting of Treacle. Thus function is strongly impaired by the K258A mutation [14]. R57D and K258R enhance (Fig. 4) and suppress (to a level intermediate between WT and K258A protein; Fig. 2), respectively, accumulation within the FC-DFC, indicating that oligomerization and ubiquitination regulate interactions with the FC-DFC. To investigate the impact of altered FC-

DFC accumulation on inhibition of rRNA biogenesis and Treacle binding, we used the Click-iT™ RNA Imaging Kit to measure rRNA biogenesis (Fig. 5A, B) and co-immunoprecipitation (co-IP) assays (Fig. 5C), as previously described [14, 23].

Consistent with previous findings, WT HeV M protein, but not HeV M K258A significantly impaired rRNA biogenesis; inhibition was consistent with that for rRNA silencing by Treacle knockdown (c. 25% inhibition) [14, 24] (Fig. 5A, B). Notably, R57D and K258R mutations significantly enhanced or impaired the inhibition of rRNA biogenesis compared to the WT protein (Fig. 5B). Consistent with the observed effects on FC-DFC targeting by K258A and K258R mutations, the effect of K258R on rRNA biogenesis was intermediate between WT and K258A.

Furthermore, co-IP and immunoblotting (IB) analysis of R57D mutated HeV M protein indicated enhanced co-precipitation of Treacle compared to that precipitated by WT HeV M protein (Fig. 5C). The K258R mutant co-precipitated lower amounts of Treacle than WT protein, but more than HeV M K258A. These results suggest that FC-DFC accumulation, Treacle binding, and the inhibition of rRNA biogenesis by the HeV M protein are correlated, indicating that FC-DFC localization and Treacle interaction are regulated by M protein ubiquitination and oligomerization. These mechanisms, in turn, play a crucial role in the viral control of rRNA production.

Loss of HeV M FC-DFC accumulation does not relate to disruption or loss of FC-DFC.

Loss of HeV M FC-DFC localization (Fig. 3) could be attributed to two possible mechanisms: (1) egress of the protein from intact FC-DFC structures, or (2) reduction of FC-DFCs through events such as fusion or disassembly/disruption of the liquid bodies. To investigate this we analysed

cellular FC-DFCs and Treacle directly by fixation and immunostaining of cells 8-72 h p.t. expressing HeV M WT, K258A, K258R, or R57D (Fig. 6A-D).

In cells expressing WT GFP-HeV M protein the appearance of FC-DFCs was similar throughout the experiment (Fig. 6A). At early time points p.t., HeV M protein strongly colocalized with Treacle in FC-DFC, but this diminished over time (indicated by reduced percentage of cells with detectable colocalization of HeV M and Treacle FC-DFCs) although multiple Treacle-enriched FC-DFCs lacking HeV M association remained detectable in nucleoli (Fig. 6A, E). Thus, HeV M protein transits through FC-DFC, where it interacts with Treacle, before egress, with no significant disruption of FC-DFC structures. As expected, HeV M K258A showed no colocalization/accumulation in Treacle FC-DFC at any time point, despite clear presence of multiple FC-DFC. HeV M K258R protein showed similar results to WT, but with more rapid egress as expected (above), and no evident loss of FC-DFC (Fig. 6C, E). By 24-48 h p.t., co-localization was barely detectable, similar to K258A (Fig. 6E). In contrast, HeV M R57D consistently exhibited clear colocalization with Treacle in all detectable FC-DFCs from 8 to 48 h p.t., with only a minor downward trend (to colocalize with FC-DFC in c. 95% of cells measured) at 72 h p.t. (Fig. 6D, E). These findings are consistent with a requirement for oligomerization for HeV M protein to egress the FC-DFC. Thus, it appears that HeV M protein transits through intact FC-DFC, with the loss of colocalization due to trafficking rather than disruption or major structural change to FC-DFC.

HeV M proteins do not affect the structure or distribution of FC-DFC.

The lack of major disruption of FC-DFC during HeV M accumulation or egress is consistent with our previous findings, including using single molecule localization microscopy (SMLM) using direct stochastic optical reconstruction microscopy (*d*STORM), that showed that HeV WT M protein accumulation in FC-DFC (24 h p.t.) does not cause gross changes to FC-DFC numbers or structure analysis of FC-DFC immunostained for Treacle [14]. Together with our data on accumulation/egress, this suggests that HeV M protein exerts dynamic effects on Treacle-dependent rRNA production primarily through specific molecular interactions rather than gross structural effects on the liquid bodies [14]. Based on the enhanced FC-DFC localization and rRNA synthesis antagonistic function of HeV M R57D, we reasoned that if any structural effects occur, they would be exaggerated by this protein. Thus, we analysed cells expressing GFP-HeV M WT, R57D, K258A, GFP alone or cells not expressing (NT), by immunostaining for Treacle and *d*STORM (Fig. 7A). As previously [14], expression of HeV M WT or K258A had no significant impact on the size of Treacle FC-DFC (Fig. 7B). Comparable results were obtained for HeV M K258R and HeV M R57D. Thus, it appears that HeV M enters FC-DFC and modulates Treacle functions directly through intermolecular interactions rather than remodelling of the LLPS structures. The duration and extent of functional modulation appears to be dependent on egress, which is regulated by ubiquitination and potentially multimerization.

DISCUSSION

Here we have found that HeV M protein dynamically transits through the FC-DFC, indicating that the previously identified translocation through the nucleus/nucleolus involves additional sub-nucleolar trafficking between LLPS structures, with multiple stages regulated by post-translational modification. This transit enables regulated interactions with Treacle and other host factors,

ultimately controlling rRNA synthesis by modulating the nucleolar DNA damage response (DDR), and influencing virus assembly and budding. To our knowledge, this study represents the first delineation of the mechanisms governing the trafficking of a viral protein within sub-nucleolar LLPS structures, and expands and refines the model for M protein trafficking. Specifically, our findings demonstrate that K258, distinct from its roles in nuclear import and export, is crucial for the localization and retention/accumulation of HeV M protein in FC-DFC.

Ubiquitination is required to retain M protein in FC-DFC such that protein unable to be ubiquitinated at K258 is rapidly exported to the GC, and subsequently accumulates in the nucleoplasm due to deficient nuclear export, which is also reported to be due to defective ubiquitination. Thus, K258 ubiquitination appears to effect (1) retention in FC-DFC, and (2) triggering of nuclear export, suggesting that a stepwise ubiquitination/de-ubiquitination pathway is required for entry and retention in FC-DFC, and interaction with Treacle (K258-ubiquitinated M protein), followed by egress from FC-DFC (de-ubiquitinated M protein) and export from the nucleolus (ubiquitinated M protein), culminating in virus budding at the plasma membrane. Moreover, our data indicate a potential role for oligomerization, possibly regulated by K258 ubiquitination[18], in coordinating these processes, thereby regulating sub-nucleolar trafficking.

Movement of proteins between LLPS structures such as nucleolar subcompartments does not use entry and exit translocation processes comparable to those of membrane-enclosed organelles, but rather depends on partitioning through physicochemical properties and interactions with resident molecules [4, 25]. This likely accounts for the poor definition of nucleolar ‘targeting sequences’ compared with NLS and NES motifs that form specific interactions with trafficking receptor

proteins (importins and exportins) [26]. Ubiquitination and oligomerization play important roles in the formation and regulation of LLPS [27, 28], and, notably, our data indicate a potential role for oligomerization, possibly regulated by ubiquitination, in coordinating M protein's interactions/localization into sub-nucleolar liquid bodies. Thus, ubiquitination/oligomerisation may alter the physicochemical properties of M protein or interactions with constituents of different nucleolar condensates, as well as affecting importin/exportin interactions and interactions at budding sites. The orchestration of ubiquitination, deubiquitination, oligomerization, and LLPS interactions may thus underlie appropriate temporal regulation of rRNA silencing, virus replication, and assembly/budding, aligning with different stages of the viral life cycle [13].

As viruses typically mimic or hijack cellular processes, our findings likely have implications beyond viral infection. The intricate regulation of M protein in multiple compartments is unlikely to have evolved solely to control cytoplasmic localization for assembly and budding. Rather, it suggests a specific coordination of sub-nuclear functions, including subversion of the DDR, where M protein appears to mimic cellular NBS1 [14]. Our findings on the regulation of sub-nucleolar partitioning of M protein, including roles of positively charged residues (typical of previously described nuclear/nucleolar targeting signals), ubiquitination and oligomerisation identifies mechanisms that may be relevant to cellular proteins that transit sub-nucleolar compartments, including those of the DDR. In the light of current advances toward therapeutic modulation of cellular and viral LLPS structures [29-32], our data also has the potential to contribute to novel antiviral approaches for currently incurable Henipavirus infection, and possibly other nucleolus-related pathologies [33, 34].

MATERIALS AND METHODS

Cell culture, transfection and treatment

HEK-293T (ATCC: CRL-3216) and HeLa (ATCC: CCL-2) cells were cultured in Dulbecco's Modified Eagle Medium (DMEM) supplemented with 10% Fetal Calf Serum (FCS), 2 mM Glutamax, 50 U/mL Penicillin, and 50 µg/mL Streptomycin. The cells were maintained at 37 °C with 5% CO_2. HeLa and HEK-293T cells were grown to 80-90% confluency before transfection using Lipofectamine 2000™ and Lipofectamine 3000™, respectively, according to the manufacturer's instructions (ThermoFisher Scientific). For free ubiquitin depletion, transfected HeLa cells were treated with 50 µM MG132 or 0.5% DMSO for control at 18 h p.t. for 6 h before CLSM imaging analysis. MG132 was purchased from Sigma (M7449-200UL) as a 10 mM ready-made solution in DMSO.

Constructs

Mammalian cell expression of N-terminal GFP tagged HeV-M (Accession Number AEB21196.1), and mutants were generated by directional cloning of the M gene cDNA into the multiple cloning site of the pEGFP-C1 vector, as previously described[17]. Site-directed mutagenesis of R57D residue was performed by applying QuickChange method, using *Pfu* DNA Polymerase from Promega. The following oligonucleotides were used to introduce the single R57D mutation: 5'-caagatctataccccaggtgcaaatgagGACaaattcaacaactacatgtacatg-3' and 3'-catgtacatgtagttgttgaatttGTCctcatttgcacctggggtatagatcttg-5'. DNA sequencing was performed to confirm the correct mutation.

Confocal laser scanning microscopy (CLSM) and image analysis

For CLSM imaging analysis, HeLa cells were seeded on 1.5 (0.17 mm) thickness glass coverslips and transfected with the indicated constructs at 80-90% confluency. Imaging was performed at the indicated time p.t. or 24 h p.t., if not specified. CLSM was conducted using a Nikon C1 inverted confocal microscope with a 60× oil immersion objective (NA 1.4) at Monash Micro Imaging Facility. Live-cell CLSM imaging was performed within a heated chamber at 37 °C.

CLSM images were analyzed using ImageJ freeware software. The mean fluorescence of the nucleus (Fn), cytoplasm (Fc), nucleolus (Fnu; whole nucleolus), FC-DFC ($F_{FC\text{-}DFC}$), GC (F_{GC}), and background fluorescence (Fb) were determined. After subtracting the background fluorescence (Fb) from all values, the nuclear to cytoplasmic (Fn/c), nucleolar to nuclear (Fnu/n), and FC-DFC to GC ($F_{FC\text{-}DFC/GC}$) fluorescence ratios were calculated. In cells where accumulation into sub-nucleolar compartments was not evident (e.g., cells expressing K258A- or K258R-mutated M protein), two distinct areas in the diffuse region of the nucleolus were selected to represent the "FC-DFC" and the "GC" for image analysis. The F_{GC} analysis was based on images captured under the same microscopy and software settings.

The percentage of cells with FC-DFC accumulation was determined by dividing the number of cells showing any nucleolus with FC-DFC ≥ 1 by the total number of cells expressing the indicated proteins in each sample. Data are presented as mean ± S.E.M. (standard error of the mean) or mean ± SD (standard deviation), as indicated in the figure legend. Statistical analysis (Student's t-test) was performed using GraphPad Prism software.

Immunofluorescence (IF)

For IF staining, cells grown on glass coverslips were washed twice gently with PBS at 24 h p.t., fixed with 4% (w/v) paraformaldehyde at room temperature (RT) for 15 min, permeabilized using 0.25% Triton X-100 (v/v in PBS) at RT for 5 min, and blocked with 1% bovine serum albumin (BSA) in PBS at RT for 1 h. The cells were then incubated with primary antibody specific to Treacle (Cat # 11003-1-AP, Proteintech) at a 1:100 dilution at RT for 1.5 h. Subsequently, cells were incubated with goat anti-rabbit 568 AlexaFluor® conjugate secondary antibody (Cat # A-11011, ThermoFisher Scientific) at a 1:1000 dilution in the dark at RT for 1.5 h. DNA staining was performed using Hoechst 33342 at a 1:2000 dilution of a 20 mM stock solution (Cat # 62249, ThermoFisher Scientific). The cells were mounted onto microscope glass slides (Lomb Scientific) using Mowiol reagent.

5-ethnyl uridine (EU) incorporation assays.

Levels of rRNA synthesis were determined using an image-based technique (Click iT® RNA Alexa Fluor 594 Imaging kit, Thermo-Fisher, Cat# C10330) as previously described [14, 23, 24, 35]. Cells were incubated for 1 h in the presence of EU before fixation in 4% paraformaldehyde at RT for 12 min and permeabilization in 0.25% Triton X-100 for 5 min at RT. Samples were processed according to the manufacturer's recommendations to label incorporated EU with Alexa Fluor 594. DNA was labeled using Hoechst 33342. Cells were imaged by CLSM to detect labeling of nascent rRNA by measuring the fluorescence intensity of Alexa Fluor 594 within nucleoli. Quantitative analysis was performed using ImageJ software to determine the mean EU fluorescence of nucleoli, which were identified using a combination of DNA, GFP, and transmitted light channels. Relative rRNA synthesis levels were determined by measuring nucleolar EU levels

of both GFP-expressing and non-expressing cells from the same sample (as an internal control) and expressed as nucleolar EU of GFP-expressing cells relative to non-expressing cells.

Immunoprecipitation (IP) and immunoblotting (IB)

HEK-293T cells were seeded in 6 cm dishes and transfected to express the indicated GFP-fused proteins. At 24 h p.t., cells were harvested and lysed in 10 mM Tris/Cl pH 7.5, 150 mM NaCl, 0.5 mM EDTA, 0.5% NP-40, and 1x Protease Inhibitor Cocktail (PIC; Sigma-Aldrich Cat#11697498001) for 20 min at 4°C. The lysate was cleared by centrifugation at 20,000 xg for 6 min at 4°C, and 10% of the supernatant was collected as the 'input' sample. The remaining lysate was incubated with GFP-Trap® magnetic beads (ChromoTek) as previously described for 45 min at 4°C on a rotary mixer [14]. The beads were then washed three times with dilution buffer (10 mM Tris/Cl pH 7.5, 150 mM NaCl, 0.5 mM EDTA, 1x PIC) and resuspended in 2x SDS-PAGE sample buffer to solubilize the proteins. The entire process from the addition of lysis buffer to the addition of 2x SDS-PAGE sample buffer was completed in less than 1.5 h to minimize degradation of Treacle, which is commonly observed (e.g. [24, 35, 36]).

Immunoprecipitates and cell lysates (input) were analyzed by SDS-PAGE and immunoblotting (IB). Proteins in IP and input samples were separated on 10% SDS-PAGE gels and transferred onto nitrocellulose membranes using the Bio-Rad Trans-Blot Turbo Transfer System according to the manufacturer's instructions. After protein transfer, the membranes were blocked in blocking buffer (5% non-fat milk in PBS with 0.1% Tween-20) at RT for 1 h, incubated with the indicated primary antibodies at RT for 2 h or at 4°C overnight on a rocker, followed by incubation with HRP-conjugated secondary antibodies (goat anti-rabbit or anti-mouse) at RT for 1 h. The

membranes were then imaged using a Gel Doc™ XR+ Gel Documentation System (Bio-Rad). The primary antibodies used for IB were anti-Treacle (Cat # 11003-1-AP, Proteintech; 1:2000), anti-GFP (Cat # 11814460001, Roche; 1:2000), and anti-β-tubulin (Cat # T8328, Sigma; 1:2000). The secondary antibodies used for IB were goat anti-rabbit (Cat # AP307P) and goat anti-mouse (Cat # AP308P) IgG HRP-conjugated antibodies (Merck Millipore).

_d_STORM imaging and analysis

HeLa cells were fixed 24 h p.t. with 4% paraformaldehyde for 10 min then permeabilized with 0.1% Triton X-100 for 10 min. Fixed cells were blocked in 2% BSA/PBS for 30 min, then stained with anti-Treacle primary antibodies (3 µg/ml, 1 h) and Alexa Fluor 647 conjugated secondary antibodies (5 µg/ml, 45 min). Samples were imaged with a switching buffer of 100 mM mercaptoethylamine (MEA) in PBS made to pH 8.5 [37]. *d*STORM imaging was performed on a home-built super-resolution set-up as previously described [37, 38]. Briefly, the setup comprised an inverted fluorescence microscope (Olympus IX81, 100X 1.49 NA TIRF objective) with an EMCCD camera (Andor iXon). Blue laser excitation (Toptica iBeam 488 nm) was used to identify GFP-positive cells. High power red laser excitation (Oxxius LaserBoxx 638 nm) was used to induce reversible photoswitching of Alexa Fluor 647 fluorophores in the fixed samples. Single molecule 'blinking' events were captured at 100 Hz for between 10,000 – 20,000 frames and processed using rapi*d*STORM [39] to render a 2D coordinate map as the super-resolved *d*STORM images of subnucleolar Treacle. For analysis, images were first smoothed in ImageJ using the Gaussian Blur function (Sigma (Radius) = 0.5) to account for single molecule localization precision error. Images were converted to 8-bit (greyscale values 2-255 threshold) then converted into binary images. Using the "Distance Map" function in ImageJ, individual subnucleolar

compartments were discretized based on pixel density by applying a threshold for greyscale values 2-255. The “Analyse Particles” function was then used to identify and measure subnucleolar compartments.

FIGURE LEGENDS

Figure 1 **Pharmacological inhibition of ubiquitination impairs FC-DFC accumulation of HeV M.** (A) Schematic of a nucleolus showing the three primary sub-compartments: fibrillar centre (FC), dense fibrillar component (DFC) and granular component (GC). The region composed of the FC and DFC compartments is referred to as the FC-DFC. (B) HeLa cells transfected to express GFP-HeV M protein were treated 18 h post transfection (p.t.) with MG132 or vehicle (DMSO) for 6 h before CLSM analysis. Representative images are shown for each condition; yellow boxes are magnified in the zoom panel. White arrowheads indicate localization of M protein to sub-nucleolar compartments consistent with FC-DFC; yellow arrowheads indicate nucleoli. Images such as those in A were analysed to determine: (C) the nuclear to cytoplasmic (Fn/c) fluorescence ratio; (D) the ratio of fluorescence of the FC-DFC to that of the GC ($F_{FC-DFC/GC}$); (E) the fluorescence intensity of the GC (F_{GC}) (arbitrary units (a.u.)),, and (F) the % of HeV M-expressing cells with apparent accumulation in FC-DFC (mean percentage ± SD from two independent assays; ≥ 73 cells for each condition). Histograms for C, D and E show mean ± S.E.M. determined from n ≥ 24 cells for each condition; data from a single assay, consistent with two independent experiments. F shows mean % +/- SD. Statistical analysis used Student's t-test; ** $p < 0.01$; **** $p < 0.0001$; n.s., not-significant.

Figure 2 **K258R mutation impacts sub-nucleolar trafficking of HeV M protein**. (A) Schematic of the HeV M protein highlighting the bipartite NLS (residues 244-258; critical basic residues are in bold and underlined) and residue K258 which can undergo ubiquitination (Ubi).

Mutations used in this study are indicated (grey boxes). (B) CLSM images of living HeLa cells expressing the indicated GFP fused proteins (24 h p.t.); for HeV M WT and K258A, images are representative of 90-100% of cells in > 29 fields of view; for K258R two major populations (each representing c. 40-60% of the population) were observed with either "WT-like" (upper panel) or "K258A-like" (lower panel) phenotype. Nucleoli are highlighted by the yellow box, which is magnified in the zoom panel. White arrowheads indicate localization to FC-DFC. (C) Images such as those in B were analysed to determine the percentage of cells with clear FC-DFC accumulation of M protein (histogram shows the percentage of M protein-expressing cells containing at least one nucleolus with evident accumulation to one or more FC-DFC (data shows mean percentage ± SD, n = 3 separate assays, each sampling ≥ 119 cells. Student's t-test with Welch's correction was used determine significance; ** $p < 0.01$.) (D) Images were analysed to determine $F_{FC\text{-}DFC/GC}$ (mean ± S.E.M., n ≥ 90 cells for each condition, from three independent assays). The two distinct populations in the K258R sample are indicated. Statistical analysis used Student's t-test; **** $p < 0.0001$.

<u>Figure 3</u> **HeV M protein accumulation in FC-DFC is reduced over time, and this is augmented by K258R mutation.** (A-C) HeLa cells transfected to express the indicated proteins were analysed live at 8, 16, 24, 48 and 72 h p.t. by CLSM. Images representative of major phenotypes are shown for each condition; yellow boxes are magnified in the zoom panel. White arrowheads indicate accumulation of M protein in FC-DFC; yellow arrowheads indicate the nucleoli. Images such as those in A-C were analysed to determine: (D) the mean percentage of M protein-expressing cells with FC-DFC accumulation in any nucleolus in the cell (mean ± SD from three independent assays, n ≥ 59 cells for each condition); (E) $F_{FC\text{-}DFC/GC}$ (mean ± S.E.M., n ≥ 55

cells for each condition over three independent assays); (F) Fn/c (mean ± S.E.M.; n ≥ 24 cells) and (G) % of cells with Fn > Fc (mean ± SD from three independent assays, n ≥ 23 cells for each condition). Statistical analysis using Student's t-test was used to compare WT and K258R values at each timepoint for D and E; * $p < 0.05$; *** $p < 0.001$; **** $p < 0.0001$; ns, not-significant.

<u>Figure 4</u> **R57D mutation enhances accumulation of HeV M in FC-DFC.** (A) CLSM images of live HeLa cells expressing the indicated proteins (24 h p.t.). Images are representative of 90-100% of cells in > 9 fields of view from a single assay and typical of ≥ 4 independent assays. Hoechst 33342 (blue) was used to identify DNA/nuclei. Nucleoli are highlighted by the yellow box, which is magnified in the zoom panel. White arrowheads indicate accumulation in FC-DFC; yellow arrowheads indicate nucleoli. (B-D) Images such as those shown in A were used to determine (B) Fn/c; (C) nucleolar to nuclear fluorescence ratio (Fnu/n; Fnu is the mean fluorescence intensity for the whole nucleolus); (D) $F_{FC\text{-}DFC/GC}$. B, C and D show mean ± S.E.M., n ≥ 24 cells for each condition. Statistical analysis used Student's t-test; ** $p < 0.01$; **** $p < 0.0001$.

<u>Figure 5</u> **Silencing of rRNA synthesis and Treacle-binding by HeV M protein/mutants correlate with FC-DFC accumulation.** (A) HeLa cells were transfected to express the indicated GFP-fused proteins before addition of EU reagent (23 h p.t.) for 1h, fixation (24 h p.t.) and labeling to detect nascent RNA (EU fluorescence) and DNA (Hoechst 33342), and imaging by CLSM. (B) Images such as those in A were used to determine EU fluorescence in the nucleoli of GFP-positive cells, relative to that in non-GFP expressing cells in the same sample (mean relative EU fluorescence ± S.E.M., n ≥ 51 cells from two independent experiments). Statistical analysis used

Student's t-test. (C) HEK-293T cells were transfected to express GFP or the indicated GFP-fused proteins prior to lysis (24 h p.t.) and IP for GFP. Cell lysate (input) and IP samples were subjected IB using the indicated antibodies.

<u>Figure 6</u> Progressive decrease in FC-DFC accumulation of M protein does not correlate with a loss of FC-DFC compartments. (A-D) HeLa cells were transfected to express the indicated proteins before fixation at 8, 16, 24, 48 and 72 h p.t. and immunostaining using anti-Treacle antibody (red) and imaging via CLSM. Hoechst 33342 (blue in Merge panel) was used to localize DNA/nuclei. Representative images are shown for each condition; yellow arrowheads indicate nucleoli; unfilled white arrowheads indicate Treacle in FC-DFC; white arrowheads indicate accumulation of M protein into FC-DFC; yellow arrows indicate colocalization of Treacle and HeV M protein in FC-DFC. (E) Images such as those in A-D were analysed to determine the percentage of expressing HeV M protein with evident colocalization of HeV M and Treacle in FC-DFC ($n \geq 23$ cells for each condition).

<u>Figure 7</u> HeV M R57D mutant does not affect the structure or distribution of Treacle-enriched FC-DFC. (A) HeLa cells expressing the indicated proteins or non-transfected (NT) were fixed and immunolabeled for Treacle before imaging using SMLM, *d*STORM. Fluorescence microscopy was used to identify cells expressing GFP/GFP-fusion proteins (green). Yellow boxes in fluorescence images show zoomed region imaged using SMLM (Zoom 1), and yellow boxes in these images show additional zoom (Zoom 2). Scale bars correspond to 5000 nm (Zoom 1) and 500 nm (Zoom 2). SMLM images such as those shown in A were used to determine (B) the area

of Treacle-enriched FC-DFC (median ± S.E.M., n ≥ 501 FC-DFC). Statistical analysis used Student's t-test; ns, not significant.

ACKNOWLEDGEMENTS

We acknowledge the facilities and technical assistance of Monash Micro Imaging (Monash University) with confocal microscopy. This study was supported by National Health and Medical (NHMRC) Research Council grants 1125704, 1160838 and 1079211 to GWM; Australian Research Council (ARC) grants DP210100998, DP150102569 to GWM., and DP170104477 to TDMB; and the Miegunyah Trust Grimwade Fellowship to GWM.

1. Boisvert FM, van Koningsbruggen S, Navascues J, Lamond AI. The multifunctional nucleolus. Nat Rev Mol Cell Biol. 2007;8(7):574-85. doi: 10.1038/nrm2184. PubMed PMID: 17519961.

2. Iarovaia OV, Minina EP, Sheval EV, Onichtchouk D, Dokudovskaya S, Razin SV, et al. Nucleolus: A Central Hub for Nuclear Functions. Trends Cell Biol. 2019;29(8):647-59. Epub 2019/06/10. doi: 10.1016/j.tcb.2019.04.003. PubMed PMID: 31176528.

3. Feric M, Vaidya N, Harmon TS, Mitrea DM, Zhu L, Richardson TM, et al. Coexisting Liquid Phases Underlie Nucleolar Subcompartments. Cell. 2016;165(7):1686-97. Epub 2016/05/24. doi: 10.1016/j.cell.2016.04.047. PubMed PMID: 27212236; PubMed Central PMCID: PMCPMC5127388.

4. Lafontaine DLJ, Riback JA, Bascetin R, Brangwynne CP. The nucleolus as a multiphase liquid condensate. Nat Rev Mol Cell Biol. 2021;22(3):165-82. Epub 2020/09/03. doi: 10.1038/s41580-020-0272-6. PubMed PMID: 32873929.

5. Hiscox JA. RNA viruses: hijacking the dynamic nucleolus. Nat Rev Microbiol. 2007;5(2):119-27. Epub 2007/01/17. doi: 10.1038/nrmicro1597. PubMed PMID: 17224921; PubMed Central PMCID: PMCPMC7097444.

6. Iarovaia OV, Ioudinkova ES, Velichko AK, Razin SV. Manipulation of Cellular Processes via Nucleolus Hijaking in the Course of Viral Infection in Mammals. Cells. 2021;10(7). Epub

2021/07/03. doi: 10.3390/cells10071597. PubMed PMID: 34202380; PubMed Central PMCID: PMCPMC8303250.

7. Rawlinson SM, Moseley GW. The nucleolar interface of RNA viruses. Cell Microbiol. 2015;17(8):1108-20. doi: 10.1111/cmi.12465. PubMed PMID: 26041433.

8. Deffrasnes C, Marsh GA, Foo CH, Rootes CL, Gould CM, Grusovin J, et al. Genome-wide siRNA Screening at Biosafety Level 4 Reveals a Crucial Role for Fibrillarin in Henipavirus Infection. PLoS Pathog. 2016;12(3):e1005478. doi: 10.1371/journal.ppat.1005478. PubMed PMID: 27010548; PubMed Central PMCID: PMCPMC4806981.

9. Monaghan P, Green D, Pallister J, Klein R, White J, Williams C, et al. Detailed morphological characterisation of Hendra virus infection of different cell types using super-resolution and conventional imaging. Virol J. 2014;11:200. doi: 10.1186/s12985-014-0200-5. PubMed PMID: 25428656; PubMed Central PMCID: PMCPMC4254186.

10. Pentecost M, Vashisht AA, Lester T, Voros T, Beaty SM, Park A, et al. Evidence for ubiquitin-regulated nuclear and subnuclear trafficking among Paramyxovirinae matrix proteins. PLoS Pathog. 2015;11(3):e1004739. doi: 10.1371/journal.ppat.1004739. PubMed PMID: 25782006; PubMed Central PMCID: PMCPMC4363627.

11. Wang YE, Park A, Lake M, Pentecost M, Torres B, Yun TE, et al. Ubiquitin-regulated nuclear-cytoplasmic trafficking of the Nipah virus matrix protein is important for viral budding. PLoS Pathog. 2010;6(11):e1001186. doi: 10.1371/journal.ppat.1001186. PubMed PMID: 21085610; PubMed Central PMCID: PMCPMC2978725.

12. Battisti AJ, Meng G, Winkler DC, McGinnes LW, Plevka P, Steven AC, et al. Structure and assembly of a paramyxovirus matrix protein. Proc Natl Acad Sci U S A. 2012;109(35):13996-4000. Epub 2012/08/15. doi: 10.1073/pnas.1210275109. PubMed PMID: 22891297; PubMed Central PMCID: PMCPMC3435216.

13. Liu YC, Grusovin J, Adams TE. Electrostatic Interactions between Hendra Virus Matrix Proteins Are Required for Efficient Virus-Like-Particle Assembly. J Virol. 2018;92(13). Epub 2018/04/27. doi: 10.1128/JVI.00143-18. PubMed PMID: 29695428; PubMed Central PMCID: PMCPMC6002731.

14. Rawlinson SM, Zhao T, Rozario AM, Rootes CL, McMillan PJ, Purcell AW, et al. Viral regulation of host cell biology by hijacking of the nucleolar DNA-damage response. Nat Commun. 2018;9(1):3057. Epub 2018/08/05. doi: 10.1038/s41467-018-05354-7. PubMed PMID: 30076298; PubMed Central PMCID: PMCPMC6076271.

15. Sun W, McCrory TS, Khaw WY, Petzing S, Myers T, Schmitt AP. Matrix proteins of Nipah and Hendra viruses interact with beta subunits of AP-3 complexes. J Virol. 2014;88(22):13099-110. doi: 10.1128/JVI.02103-14. PubMed PMID: 25210190; PubMed Central PMCID: PMCPMC4249102.

16. Donnelly CM, Vogel OA, Edwards MR, Taylor PE, Roby JA, Forwood JK, et al. Henipavirus Matrix Protein Employs a Non-Classical Nuclear Localization Signal Binding Mechanism. Viruses. 2023;15(6). Epub 2023/06/28. doi: 10.3390/v15061302. PubMed PMID: 37376602; PubMed Central PMCID: PMCPMC10303457.

17. McLinton EC, Wagstaff KM, Lee A, Moseley GW, Marsh GA, Wang LF, et al. Nuclear localization and secretion competence is conserved amongst henipavirus matrix proteins. J Gen Virol. 2017. doi: 10.1099/jgv.0.000703. PubMed PMID: 28056216.

18. Watkinson RE, Lee B. Nipah virus matrix protein: expert hacker of cellular machines. FEBS Lett. 2016;590(15):2494-511. doi: 10.1002/1873-3468.12272. PubMed PMID: 27350027.

19. Liang SH, Clarke MF. Regulation of p53 localization. Eur J Biochem. 2001;268(10):2779-83. Epub 2001/05/19. doi: 10.1046/j.1432-1327.2001.02227.x. PubMed PMID: 11358492.

20. Gorby C, Martinez-Fabregas J, Wilmes S, Moraga I. Mapping Determinants of Cytokine Signaling via Protein Engineering. Front Immunol. 2018;9:2143. Epub 2018/10/16. doi: 10.3389/fimmu.2018.02143. PubMed PMID: 30319612; PubMed Central PMCID: PMCPMC6170656.

21. Banani SF, Lee HO, Hyman AA, Rosen MK. Biomolecular condensates: organizers of cellular biochemistry. Nat Rev Mol Cell Biol. 2017;18(5):285-98. Epub 2017/02/23. doi: 10.1038/nrm.2017.7. PubMed PMID: 28225081; PubMed Central PMCID: PMCPMC7434221.

22. Boeynaems S, Alberti S, Fawzi NL, Mittag T, Polymenidou M, Rousseau F, et al. Protein Phase Separation: A New Phase in Cell Biology. Trends Cell Biol. 2018;28(6):420-35. Epub 2018/04/01. doi: 10.1016/j.tcb.2018.02.004. PubMed PMID: 29602697; PubMed Central PMCID: PMCPMC6034118.

23. Rawlinson SM, Zhao T, Ardipradja K, Zhang Y, Veugelers PF, Harper JA, et al. Henipaviruses and lyssaviruses target nucleolar treacle protein and regulate ribosomal RNA

synthesis. Traffic. 2023;24(3):146-57. Epub 2022/12/09. doi: 10.1111/tra.12877. PubMed PMID: 36479968.

24. Larsen DH, Hari F, Clapperton JA, Gwerder M, Gutsche K, Altmeyer M, et al. The NBS1-Treacle complex controls ribosomal RNA transcription in response to DNA damage. Nat Cell Biol. 2014;16(8):792-803. doi: 10.1038/ncb3007. PubMed PMID: 25064736; PubMed Central PMCID: PMCPMC4962910.

25. Ditlev JA, Case LB, Rosen MK. Who's In and Who's Out-Compositional Control of Biomolecular Condensates. J Mol Biol. 2018;430(23):4666-84. Epub 2018/08/14. doi: 10.1016/j.jmb.2018.08.003. PubMed PMID: 30099028; PubMed Central PMCID: PMCPMC6204295.

26. Emmott E, Hiscox JA. Nucleolar targeting: the hub of the matter. EMBO Rep. 2009;10(3):231-8. doi: 10.1038/embor.2009.14. PubMed PMID: 19229283; PubMed Central PMCID: PMCPMC2658561.

27. Luo YY, Wu JJ, Li YM. Regulation of liquid-liquid phase separation with focus on post-translational modifications. Chem Commun (Camb). 2021;57(98):13275-87. Epub 2021/11/25. doi: 10.1039/d1cc05266g. PubMed PMID: 34816836.

28. Mohanty P, Kapoor U, Sundaravadivelu Devarajan D, Phan TM, Rizuan A, Mittal J. Principles Governing the Phase Separation of Multidomain Proteins. Biochemistry. 2022. Epub 2022/07/09. doi: 10.1021/acs.biochem.2c00210. PubMed PMID: 35802394.

29. Conti BA, Oppikofer M. Biomolecular condensates: new opportunities for drug discovery and RNA therapeutics. Trends Pharmacol Sci. 2022;43(10):820-37. Epub 2022/08/27. doi: 10.1016/j.tips.2022.07.001. PubMed PMID: 36028355.

30. Mitrea DM, Mittasch M, Gomes BF, Klein IA, Murcko MA. Modulating biomolecular condensates: a novel approach to drug discovery. Nat Rev Drug Discov. 2022;21(11):841-62. Epub 2022/08/17. doi: 10.1038/s41573-022-00505-4. PubMed PMID: 35974095; PubMed Central PMCID: PMCPMC9380678 discovery company that studies condensates, and have a financial stake in the company.

31. Risso-Ballester J, Galloux M, Cao J, Le Goffic R, Hontonnou F, Jobart-Malfait A, et al. A condensate-hardening drug blocks RSV replication in vivo. Nature. 2021;595(7868):596-9. Epub 2021/07/09. doi: 10.1038/s41586-021-03703-z. PubMed PMID: 34234347.

32. Wang S, Dai T, Qin Z, Pan T, Chu F, Lou L, et al. Targeting liquid-liquid phase separation of SARS-CoV-2 nucleocapsid protein promotes innate antiviral immunity by elevating MAVS activity. Nat Cell Biol. 2021;23(7):718-32. Epub 2021/07/10. doi: 10.1038/s41556-021-00710-0. PubMed PMID: 34239064.

33. Maehama T, Nishio M, Otani J, Mak TW, Suzuki A. Nucleolar stress: Molecular mechanisms and related human diseases. Cancer Sci. 2023;114(5):2078-86. Epub 2023/02/11. doi: 10.1111/cas.15755. PubMed PMID: 36762786; PubMed Central PMCID: PMCPMC10154868.

34. Stochaj U, Weber SC. Nucleolar Organization and Functions in Health and Disease. Cells. 2020;9(3). Epub 2020/02/29. doi: 10.3390/cells9030526. PubMed PMID: 32106410; PubMed Central PMCID: PMCPMC7140423.

35. Mooser C, Symeonidou IE, Leimbacher PA, Ribeiro A, Shorrocks AK, Jungmichel S, et al. Treacle controls the nucleolar response to rDNA breaks via TOPBP1 recruitment and ATR activation. Nat Commun. 2020;11(1):123. Epub 2020/01/09. doi: 10.1038/s41467-019-13981-x. PubMed PMID: 31913317; PubMed Central PMCID: PMCPMC6949271.

36. Ciccia A, Huang JW, Izhar L, Sowa ME, Harper JW, Elledge SJ. Treacher Collins syndrome TCOF1 protein cooperates with NBS1 in the DNA damage response. Proc Natl Acad Sci U S A. 2014;111(52):18631-6. doi: 10.1073/pnas.1422488112. PubMed PMID: 25512513; PubMed Central PMCID: PMCPMC4284564.

37. Whelan DR, Bell TD. Image artifacts in single molecule localization microscopy: why optimization of sample preparation protocols matters. Sci Rep. 2015;5:7924. doi: 10.1038/srep07924. PubMed PMID: 25603780; PubMed Central PMCID: PMCPMC4300460.

38. Rozario AM, Zwettler F, Duwé S, Hargeaves RB, Brice A, Dedecker P, et al. 'Live and large': super-resolution optical fluctuation imaging (SOFI) and expansion microscopy (ExM) of microtubule remodelling by rabies virus P protein. Aust J Chem. 2020;73(8):686-92.

39. Wolter S, Loschberger A, Holm T, Aufmkolk S, Dabauvalle MC, van de Linde S, et al. rapidSTORM: accurate, fast open-source software for localization microscopy. Nat Methods. 2012;9(11):1040-1. doi: 10.1038/nmeth.2224. PubMed PMID: 23132113.

Figure 1

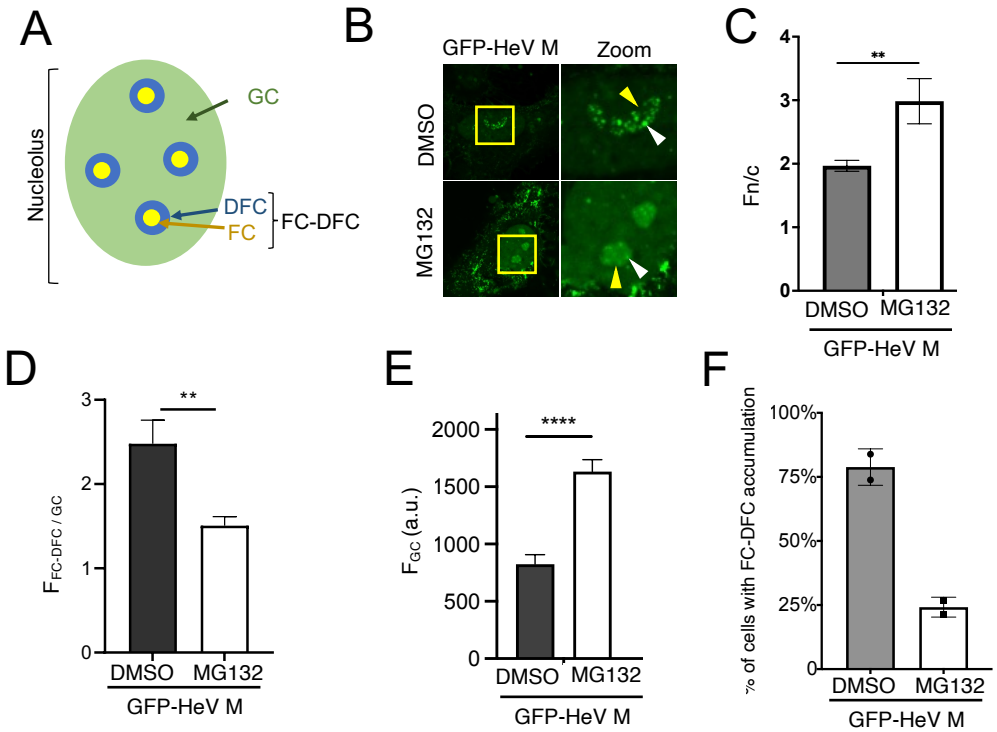
A
Nucleolus
GC
DFC
FC
FC-DFC
B
GFP-HeV M
Zoom
DMSO
MG132
C
Fn/c
**
DMSO
MG132
GFP-HeV M
D
$F_{FC-DFC / GC}$
**
DMSO
MG132
GFP-HeV M
E
F_{GC} (a.u.)
****
DMSO
MG132
GFP-HeV M
F
% of cells with FC-DFC accumulation
100%
75%
50%
25%
DMSO
MG132
GFP-HeV M

Figure 2

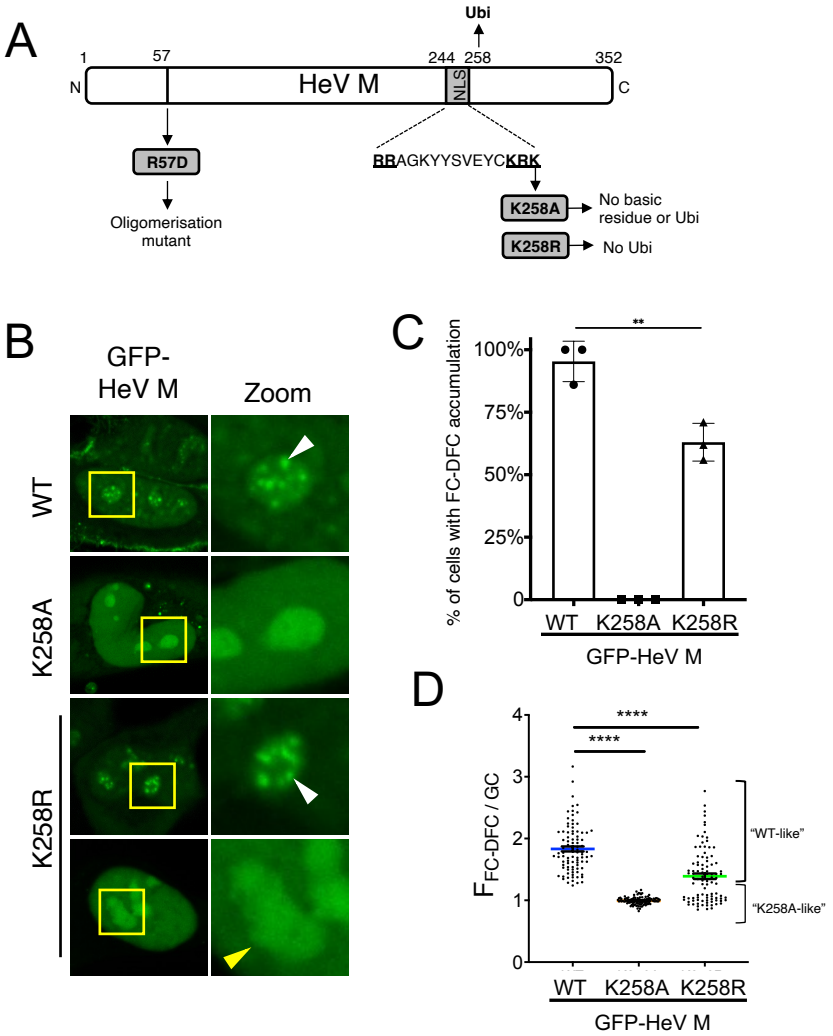
A
Ubi
1
57
244
258
352
N
HeV M
NLS
C
R57D
Oligomerisation mutant
RRAGKYYSVEYCKRK
K258A
No basic residue or Ubi
K258R
No Ubi
B
GFP-HeV M
Zoom
WT
K258A
K258R
C
% of cells with FC-DFC accumulation
100%
75%
50%
25%
0
**
WT
K258A
K258R
GFP-HeV M
D
F_{FC-DFC} / GC
4
3
2
1
0
****
****
"WT-like"
"K258A-like"
WT
K258A
K258R
GFP-HeV M

Figure 3

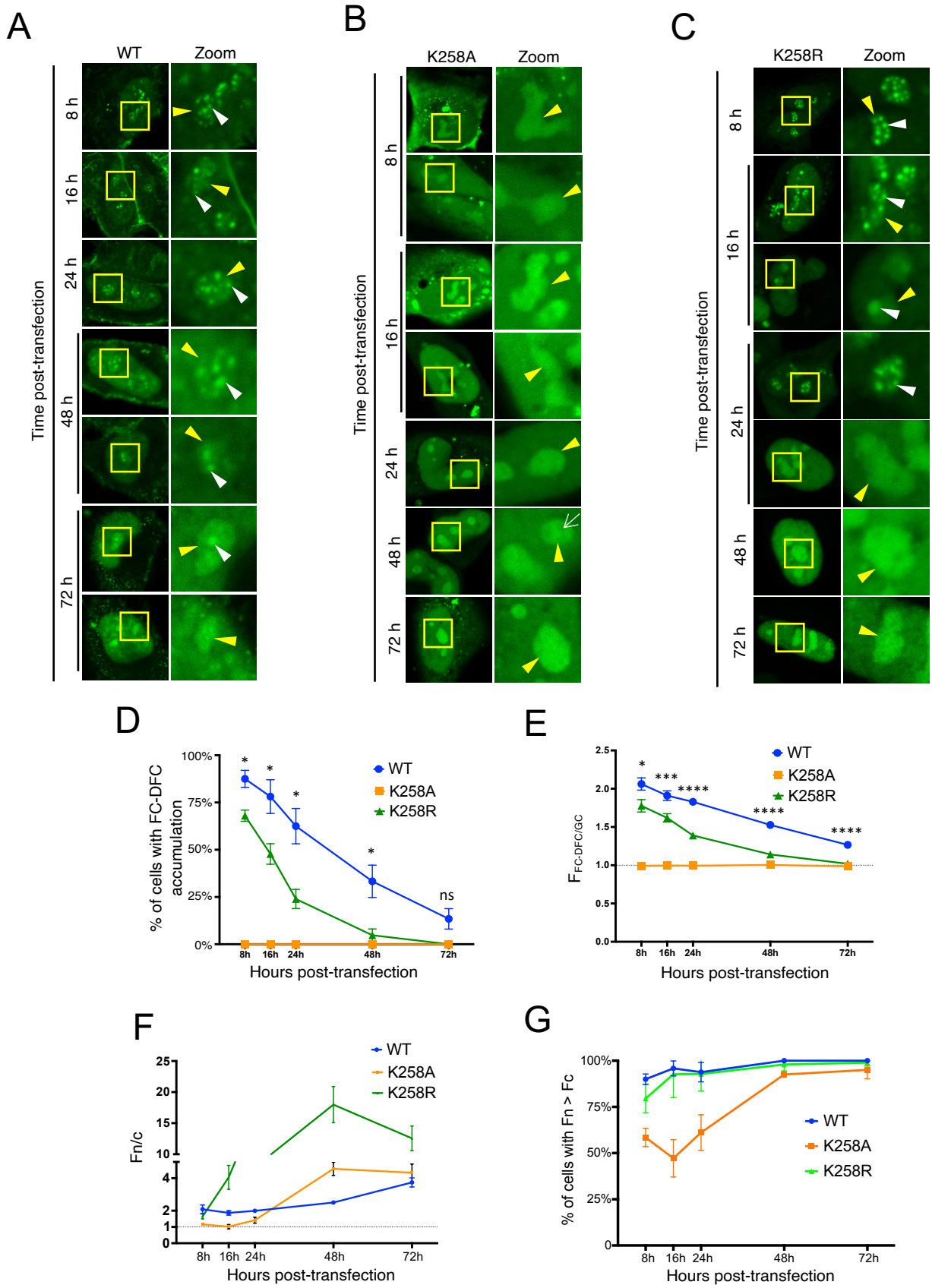
A
WT
Zoom
Time post-transfection
8 h
16 h
24 h
48 h
72 h
B
K258A
Zoom
C
K258R
Zoom
D
% of cells with FC-DFC accumulation
100%
75%
50%
25%
0%
WT
K258A
K258R
ns
8h
16h
24h
48h
72h
Hours post-transfection
E
$F_{FC\text{-}DFC/GC}$
2.5
2.0
1.5
1.0
0.5
0.0
***
****
F
Fn/c
25
20
15
10
4
2
1
0
G
% of cells with Fn > Fc

Figure 4

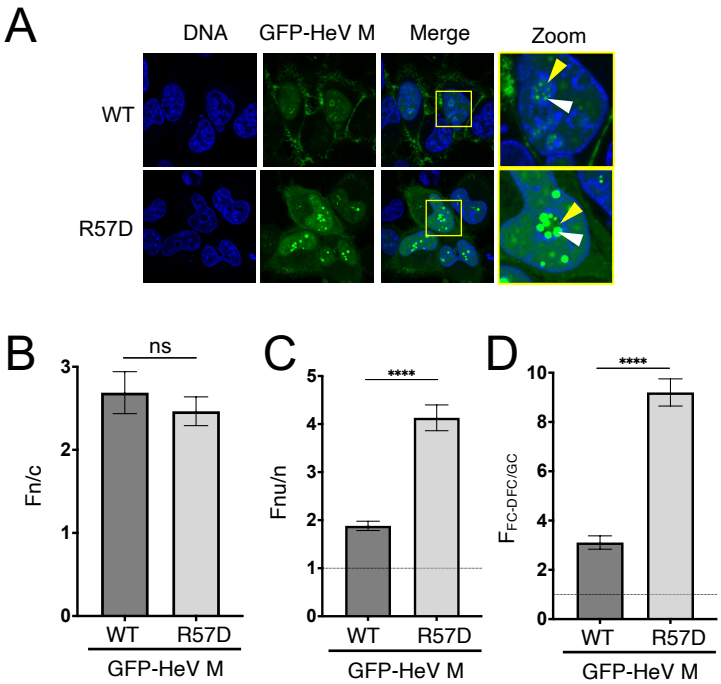
A
DNA
GFP-HeV M
Merge
Zoom
WT
R57D
B
ns
Fn/c
3
2
1
0
WT
R57D
GFP-HeV M
C
****
Fnu/n
5
4
3
2
1
0
WT
R57D
GFP-HeV M
D
****
$F_{FC-DFO/GC}$
10
8
6
4
2
0
WT
R57D
GFP-HeV M

Figure 5

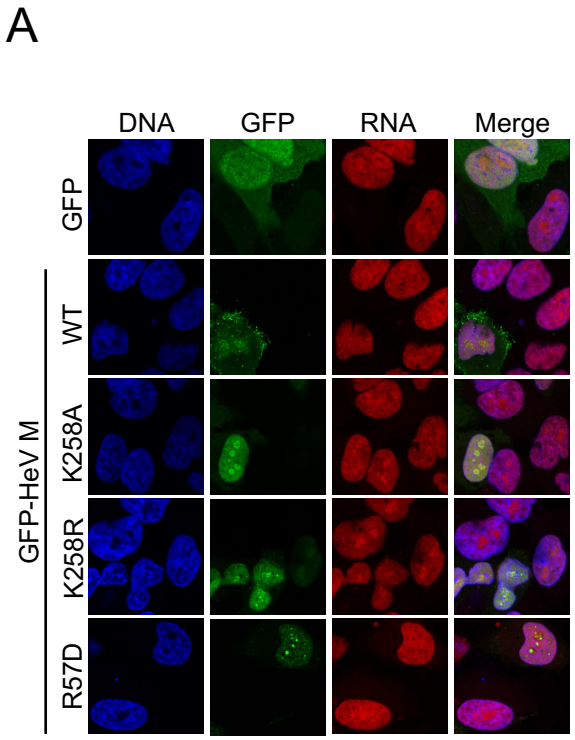
A
DNA
GFP
RNA
Merge
GFP
GFP-HeV M
WT
K258A
K258R
R57D

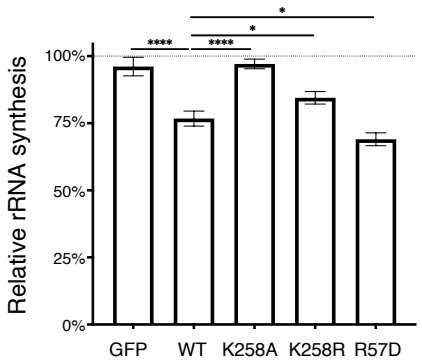
B
Relative rRNA synthesis
100%
75%
50%
25%
0%
****
****
*
*
GFP
WT
K258A
K258R
R57D

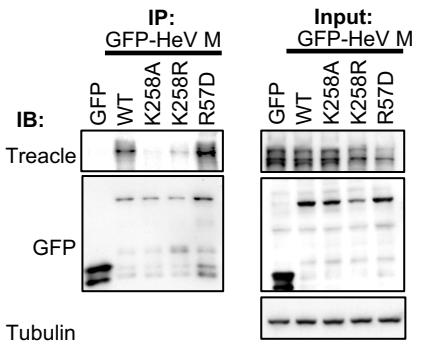
C
IP:
GFP-HeV M
Input:
GFP-HeV M
IB:
GFP
WT
K258A
K258R
R57D
Treacle
GFP
Tubulin

Figure 6

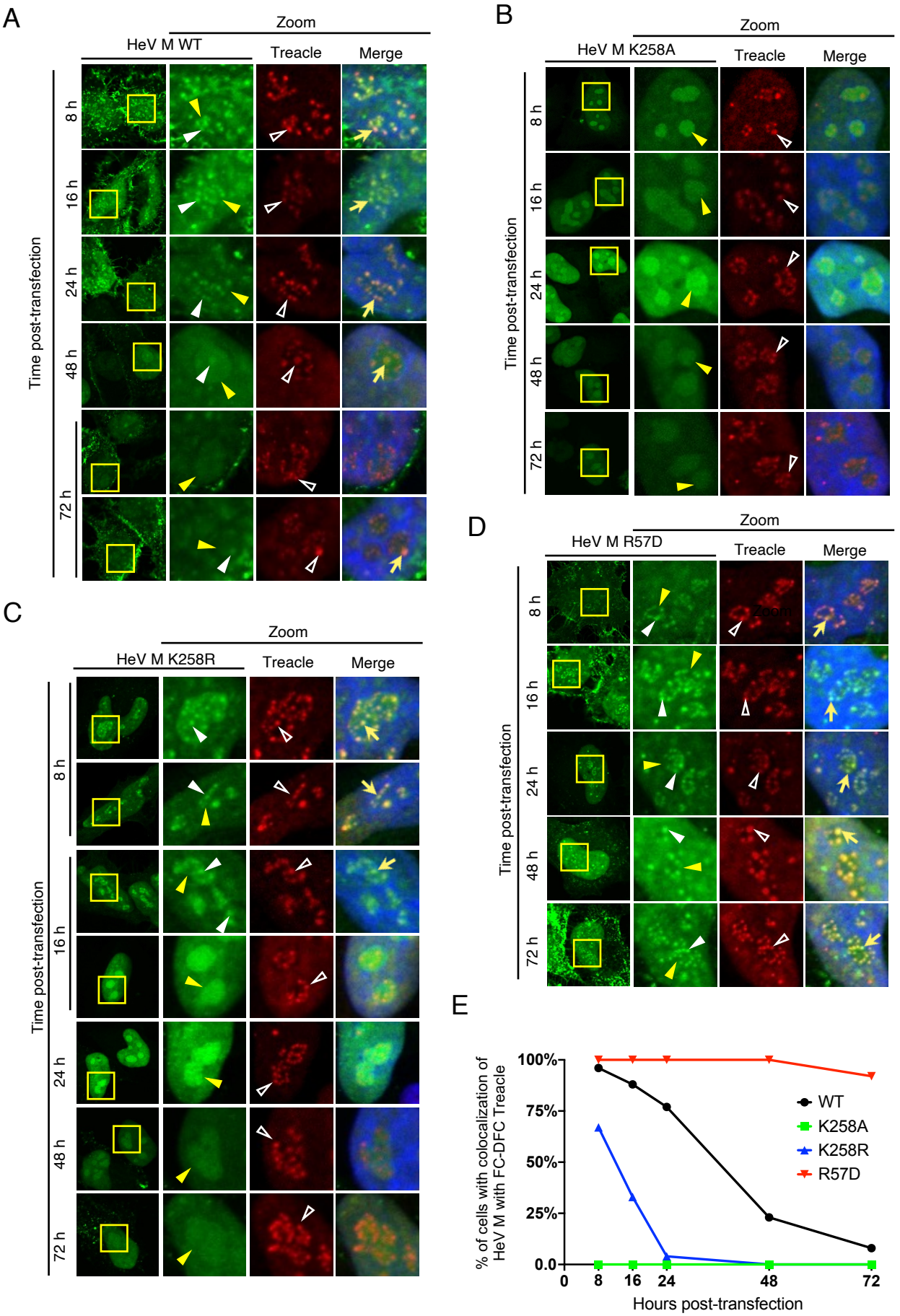
A
Zoom
HeV M WT
Treacle
Merge
Time post-transfection
8 h
16 h
24 h
48 h
72 h
B
Zoom
HeV M K258A
Treacle
Merge
Time post-transfection
8 h
16 h
24 h
48 h
72 h
C
Zoom
HeV M K258R
Treacle
Merge
Time post-transfection
8 h
16 h
24 h
48 h
72 h
D
Zoom
HeV M R57D
Treacle
Merge
Time post-transfection
8 h
16 h
24 h
48 h
72 h
E
% of cells with colocalization of HeV M with FC-DFC Treacle
100%
75%
50%
25%
0.0
0
8
16
24
48
72
Hours post-transfection
WT
K258A
K258R
R57D

Figure 7

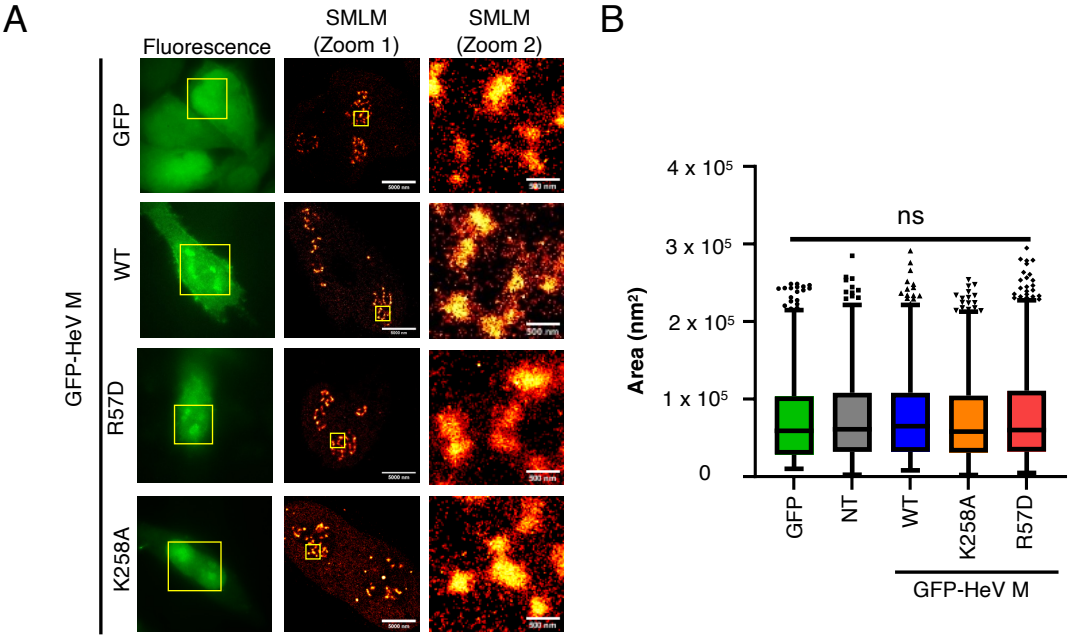
A
Fluorescence
SMLM (Zoom 1)
SMLM (Zoom 2)
GFP-HeV M
GFP
WT
R57D
K258A
B
Area (nm²)
4 x 10⁵
3 x 10⁵
2 x 10⁵
1 x 10⁵
0
ns
GFP
NT
WT
K258A
R57D
GFP-HeV M